Chem

CellPress
OPEN ACCESS

Article

Understanding radiative transitions and relaxation pathways in plexcitons

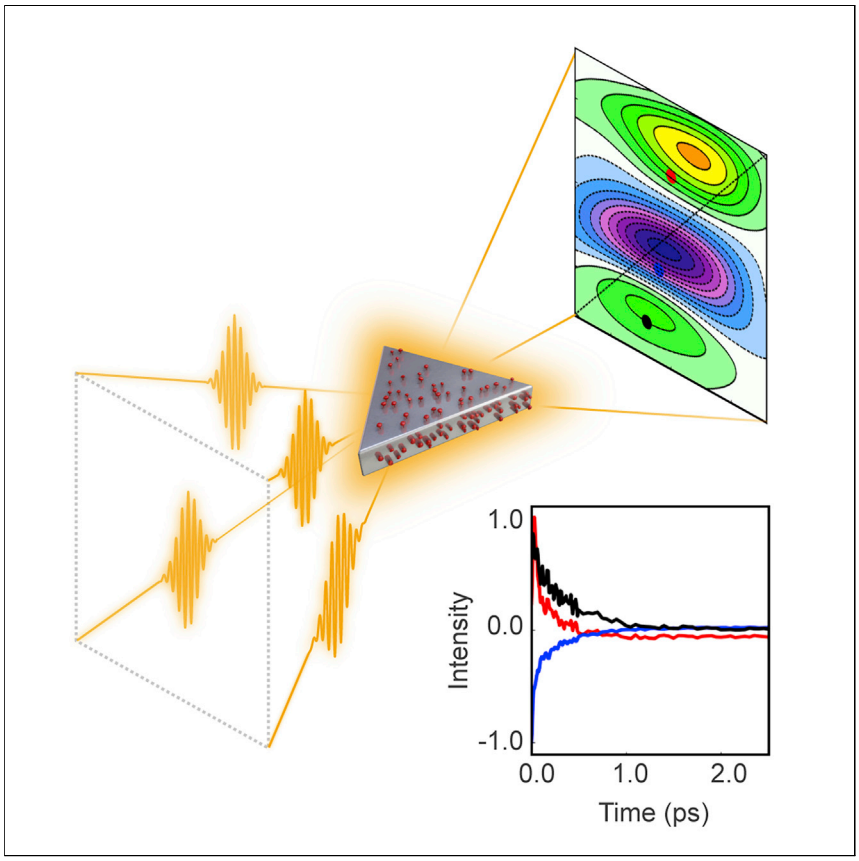

When molecules are close to plasmonic nanoparticles, they form hybridized light-matter or plexciton states. Potential use of plexcitonic materials depends on their coherence and excitation lifetimes, and thus, it is important to identify their limiting factors. We combine theoretical modeling with multidimensional spectroscopy to study relaxation of plexciton states from a few femtoseconds to their thermalization. This enables us to assign responsible physical mechanisms and provide an understanding on which to base further improvements of the materials.

Daniel Finkelstein-Shapiro, Pierre-Adrien Mante, Sema Sarisozen, ..., Sinan Balci, Tõnu Pullerits, Donatas Zigmantas

daniel.finkelstein@iquimica.unam.mx (D.F.-S.)
donatas.zigmantas@chemphys.lu.se (D.Z.)

Highlights

Identification of theoretical formalism for calculating plexciton optical properties

Assignment of various dissipation mechanisms in hybrid plexciton materials

Recognition of limitations on coherence and energy lifetimes in plexcitons

Finkelstein-Shapiro et al., Chem 7, 1092–1107
April 8, 2021
https://doi.org/10.1016/j.chempr.2021.02.028

CellPress
OPEN ACCESS

Chem

Article

Understanding radiative transitions and relaxation pathways in plexcitons

Daniel Finkelstein-Shapiro,[1,4,*] Pierre-Adrien Mante,[1] Sema Sarisozen,[2] Lukas Wittenbecher,[1] Iulia Minda,[1] Sinan Balci,[3] Tõnu Pullerits,[1] and Donatas Zigmantas[1,5,*]

SUMMARY

Molecular aggregates on plasmonic nanoparticles have emerged as attractive systems for the studies of polaritonic light-matter states, called plexcitons. Such systems are tunable, scalable, easy to synthesize, and offer sub-wavelength confinement, all while giving access to the ultrastrong light-matter coupling regime, promising a plethora of applications. However, the complexity of these materials prevented the understanding of their excitation and relaxation phenomena. Here, we follow the relaxation pathways in plexcitons and conclude that while the metal destroys the optical coherence, the molecular aggregate coupled to surface processes significantly contributes to the energy dissipation. We use two-dimensional electronic spectroscopy with theoretical modeling to assign the different relaxation processes to either molecules or metal nanoparticle. We show that the dynamics beyond a few femtoseconds has to be considered in the language of hot electron distributions instead of the accepted lower and upper polariton branches and establish the framework for further understanding.

INTRODUCTION

Cavity quantum electrodynamics (cQED) has been a very successful testbed for the quantum mechanics of light-matter interaction,[1–4] and exhibits phenomena of both fundamental and practical interest.[5–16] Dressing matter with the electromagnetic modes of a cavity results in hybrid light-matter states (polaritons) with properties that are only recently beginning to be exploited for chemistry applications, such as photocatalysis,[17,18] remote energy transfer,[11,19–24] and polaritonic chemistry.[25–28] As the light-matter coupling strength increases, new and unexpected effects arise tied to non-zero ground-state occupation of the cavity, so that finding systems that can push the coupling into stronger regimes are desirable to explore new photophysics and photochemistry.[29–31] Condensed-matter cQED realizations are particularly attractive as they reach the ultrastrong coupling regime at room temperature, with Rabi splittings in excess of 30%, as compared with the emitter frequency.[1,14,32–40] This regime can be reached both by molecules placed in a microcavity,[14,31] or in systems where the field has been confined by a plasmonic resonance to sub-wavelength dimensions, as is the case for plexcitons (plasmon + exciton).[30,38] Confining the light mode in a plasmonic nanoparticle, as opposed to a microcavity or a plasmonic array, provides a notable advantage: the systems can be synthesized in large numbers using synthetic chemistry methods, and exist as colloidal suspensions in solution. Thus, they provide polaritonic states in a beaker.

The bigger picture

Polaritonic (light + matter) states have gathered broad interests owing to their ability to modify the molecular energy landscape by using strong coupling to an electromagnetic mode. There are now many proof-of-concept applications showcasing their usefulness in controlling energy harvesting and chemical reactions. Plexcitons, where the plasmon in metallic nanoparticle is coupled to the molecules, are advantageous because they can be made in large numbers using simple chemistry methods. There is, however, a limited understanding of the nature of excitations and the mechanisms of energy dissipation in these materials. We used multidimensional spectroscopy with simulations to provide the lacking understanding of these properties. We found that energy dissipation is highly complex but could be potentially tuned. Our study on fundamental properties of plexcitons is a necessary stepping stone toward a much broader research program to find applications of these materials for the society at large.

There is an increasing complexity of the dissipative environment in polaritonic systems as we move from atoms to molecules in microcavities, and finally to molecules coupled to plasmonic nanoparticles. The wealth of dissipative processes when replacing a cavity with a plasmon—for example, Landau damping, electron-electron (e-e) scattering and electron-phonon (e-ph) scattering—modulate the dynamics in non-trivial ways that cannot be ignored.[41] A stronger coupling to a dissipative environment, however, needs not be necessarily detrimental, and there are several examples where harnessing it increases device efficiency, and therefore dissipation should be understood and explored.[42,43]

Ultrafast pump-probe studies have reported the relaxation times of the excitation[44–49] as well as the Rabi oscillations in the case of molecules coupled to gold nanoslit arrays.[47] Unfortunately, currently there is no consensus on the plexciton lifetimes and dephasing processes, likely stemming from system to system differences, and non-trivial excitation wavelength dependence. For example, Hranisavljevic et al. found an exceptionally stabilized excited state with a 300 ps decay constant,[46] while Balci et al. measured decay constants close to 10 ps, which are pump wavelength dependent,[45] in similar systems consisting of cyanine dyes adsorbed on Ag plasmonic nanoparticles. More importantly, an understanding of the dissipation in terms of the physical mechanisms in the molecular aggregates or the plasmonic nanoparticles is lacking, so that rational and systematic improvements of these materials are hindered. The studies of microcavity polaritons in the infrared region (where molecular vibrations are dressed by the cavity modes) are more mature, and can provide useful guidelines as to what differences we might expect between molecular and atomic systems.[50] Notably, previous studies underscore the importance of dark states,[50,51] although extrapolating the same physics to plasmonic-based hybrids in the visible regime should be done with care. Recent transient absorption studies at visible wavelengths find that two-particle polaritonic states play an important role,[52] while a two-dimensional electronic spectroscopy (2DES) investigation has measured a relaxation pathway from upper to lower branch without the involvement of the molecular dark states.[53]

In this work, we explored the ultrafast dynamics of plexcitons and corresponding dissipation mechanisms in detail. We started from a description of the plexciton linear absorption by extending the response function formalism to non-Hermitian Hamiltonians. This formed the basis to interpret 2DES experiments and to propose a physical origin of each relaxation component observed in the plexciton, either to processes inside the J-aggregates or inside the metal nanoparticle.

RESULTS

J-aggregates (TDBC, 5,5,6,6-tetrachloro-di(4-sulfobutyl) benzimidazolocarbocyanine), Ag nanoprisms, and plexcitons (TDBC-Ag nanoprism) were prepared as reported previously (see Experimental procedures section.[38,54]). The samples were prepared in solution and all non-linear spectroscopy measurements were done in transmission mode.

Linear response

The absorption spectrum can be used to infer the homogeneous linewidth (when it is much larger than the heterogeneous broadening) and the energy structure of the first excited-state manifold (Figure 1A), a prerequisite to correctly interpret the third-order response signals presented below. The absorption spectrum of the plexciton clearly shows the upper and lower polaritonic branches (Figure 1B). The minimum of the dip in the spectrum is nearly coincident with the J-aggregate absorption at 16,950 cm^{-1} (590 nm).

[1]Division of Chemical Physics and Nanolund, Lunds Universitet, 221 00 Lund, Sweden

[2]Department of Chemistry, Izmir Institute of Technology, 35430 Izmir, Turkey

[3]Department of Photonics, Izmir Institute of Technology, 35430 Izmir, Turkey

[4]Present address: Instituto de Química, Universidad Nacional Autónoma de México, 04510 Ciudad de México, México

[5]Lead contact

*Correspondence: daniel.finkelstein@iquimica.unam.mx (D.F.-S.), donatas.zigmantas@chemphys.lu.se (D.Z.)

https://doi.org/10.1016/j.chempr.2021.02.028

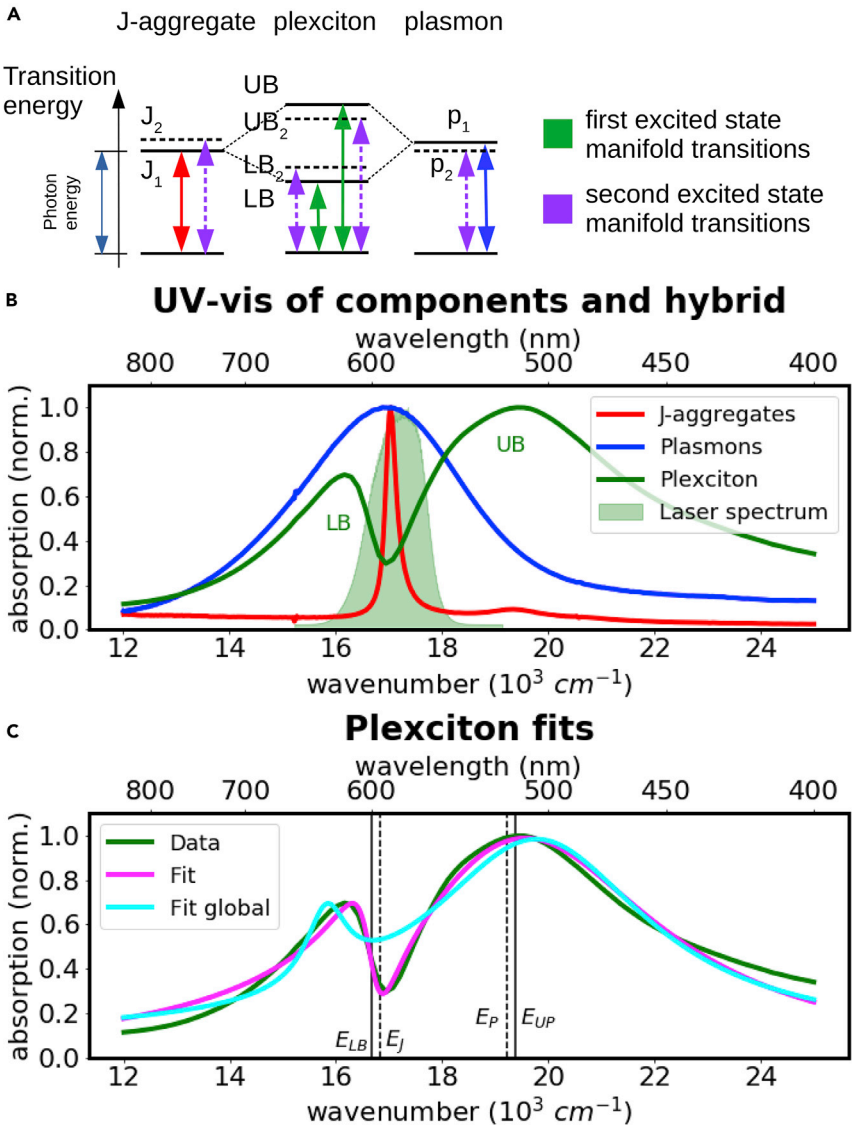

Figure 1. Linear optical response

(A) Transition energy of the ground to first and from the first to the second exciton manifolds. In plexcitons, matter and light states hybridize to give a lower and upper polaritonic branch. The nonlinearity shown between the first to second exciton manifold transition compared with the ground to first exciton manifold transition is due to a Rabi contraction. We neglected the transitions to higher electronic states lying two photon quanta above the ground state, since their contribution is much smaller than double excitations of the levels lying one photon above the ground state.

(B) Absorption spectrum of J-aggregates and extinction spectrum of plasmons and plexcitons, with the laser spectrum of the pulses used in 2DES experiments.

(C) The measured and fitted plexciton extinction spectra using the local and global approaches (see main text). Dashed vertical lines indicate the uncoupled J-aggregate and plasmon transition frequencies, while solid lines indicate the upper and lower polariton transition frequencies (we use $\omega = 2\pi\tilde{\nu}c$).

Next, through the fitting of the line shape, we obtained the energy and dephasing time of the first excited states manifold and motivate the structure of the higher excited states manifold based on previous measurements and theoretical models (Figure 1A; Agranovich and Malshukov[55] and Minoshima et al.[56]) An ideal J-aggregate consisting of N monomers with individual transition dipole moments μ_0

features a single bright exciton state carrying all of the transition dipole moment strength $\mu_{bright} = \sqrt{N}\mu_0$, and $N-1$ dark states. Although this is strictly true only in the absence of disorder, its predictions are in agreement with the absorption spectrum of the J-aggregate consisting of a very strong and narrow absorption line. It is well fit by a Lorentzian with center frequency $\tilde{\nu}_{J_1} = 17.04\times10^3$ cm^{-1} and full width at half maximum (FWHM) of $\gamma_{J_1} = 120$ cm^{-1}, corresponding to a dephasing time of 44 fs (Figure S1). The double exciton states manifold consists of a band whose transition from the first exciton manifold ($1\rightarrow2$) is almost isoenergetic with the first transition ($0\rightarrow1$),[57] and its detuning can be calculated from the linear Frenkel exciton model.[56] While both first and second excited states form bands, we will refer to them as single states under the viewpoint that most of the transition dipole moment strength is carried by one state. Analogous to the J-aggregate transition, we model the line shape of the plasmon absorption in the Ag nanoparticles as a Lorentzian with center wavenumber $\tilde{\nu}_{p_1} = 16.92\times10^3$ cm^{-1} and a width of $\gamma_{p_1} = 1.78\times10^3$ cm^{-1} corresponding to a dephasing time of 3 fs (Figure S2).

Given the electronic structure of the individual components, and the expected coupling between them, we arrived at the energy level structure shown in Figure 1A. We summarize the state energies and couplings in the following Hamiltonian, which is analogous to that proposed by others[58–62] (see Figure 1A). The Hamiltonian in the $\{g, p_1, J_1\}$ basis (that we call here site basis) reads:

$$H_{site} = \begin{bmatrix} 0 & F\mu_{gp_1} & F\mu_{gJ_1} \\ F\mu_{p_1g} & \hbar\bar{\omega}_{p_1} & V_1 \\ F\mu_{J_1g} & V_1^* & \hbar\bar{\omega}_{J_1} \end{bmatrix} \qquad \text{(Equation 1)}$$

where $\bar{\omega}_j = \omega_j - i\gamma_j$ is a complex frequency that accounts for the transition frequency ω_j and its associated dephasing rate γ_j, μ_{ji} are the transition dipole moments from i to j, F is the field strength and V_i is the dipolar coupling between the J-aggregate and the plasmon's ith excited state. g is the shared ground state, and p_i and J_i are the ith excited state of the plasmon and J-aggregate, respectively (the measured spectra are displayed in wavenumbers $\tilde{\nu} = \omega/(2\pi c)$, where ω is the angular frequency and c is the speed of light). The second excitations of the individual components are also labeled in Figure 1A.

In order to use the same theoretical approach for the linear and third-order response, we simulated the absorption spectrum using the response function formalism[63] with two different limits of the Markovian bath.[64] In the polariton basis—obtained by diagonalizing H_{site} at zero-field ($F = 0$) and without including the dephasing (that is setting $\bar{\omega}_j = \omega_j$)—we could express the linear absorption as a sum over polariton state contributions[65,66]:

$$I(\omega) = \int dt e^{i\omega t} \sum_{a=\mathrm{UB,LB}} \mu_{ga}^{(g)}\mu_{ag}^{(g)} e^{\left(-i\left(\omega_a^{(g)}-\omega_g\right)-\gamma_a^{(g)}\right)t}, \qquad \text{(Equation 2)}$$

where $\mu_{ag}^{(g)}$, $\omega_a^{(g)}$, and $\gamma_a^{(g)}$ are the transition dipole moment from level g to the polaritonic upper or lower branch $a\in\{LB, UB\}$, the transition frequency between g and a and the dephasing rate, respectively. The (g) or (l) (used below) superscript refer to the global and local approach taken to obtain the polariton branches. In the global approach, the transition frequencies and transition dipole moments are obtained from the diagonalization of the Hamiltonian without dephasing, with the dephasing rate of each branch introduced phenomenologically in the expression for the absorption (Equation 2). This model fits the spectrum poorly (cyan, Figure 1C).

The global approach model is equivalent to fitting the absorption spectrum to a sum of Lorentzians (here two) that in this case do not correspond to the line shape measured. We instead diagonalized the non-Hermitian operator H_{site}, including the dephasing rates $\gamma_{J_1}, \gamma_{p_1}$ (as the imaginary part of the transition frequencies) to obtain the new (complex) polariton branch energies $\omega_a^{(l)}$ and their respective transition dipole moments $\mu_{ag}^{(l)}$. We modified the expression for the linear response accordingly to:

$$I(\omega) = \int dt e^{i\omega t} \sum_{a=UB,LB} \mu_{ga}^{(l)} \mu_{ag}^{(l)} e^{-i\left(\omega_a^{(l)} - \omega_g^*\right)t}, \qquad \text{(Equation 3)}$$

so that the dephasing rates are included in the complex energies of the polaritonic states. As we see from Figure 1C, in the local approach fit (magenta line) the agreement with the model is excellent, with deviations attributable to the simplifying assumption of representing the plasmon line shape by a Lorentzian far away from the resonance (Figure S2). The name of the models (local versus global) refer to the approximations implemented to reach the underlying Markovian master equation,[64] and a more detailed discussion of their physical meaning can be found in Note S1.

The parameters of the fits are reported in Table 1, assuming that the principal contribution to the resonance width is homogeneous broadening. The plasmon dephasing time was extremely fast (1.6 fs), in agreement with previous measurements.[67,68] This fast dephasing rate was inherited to the plexcitonic branches (1.7 and 15 fs for upper and lower branch, respectively). The difference in dephasing rates can be attributed to the upper branch having more of a plasmonic character than the lower branch. This is clear from detuning between the plasmon (19.22×10^3 cm^{-1}) and the J-aggregate transition (16.83×10^3 cm^{-1}). The frequencies of the radiative transition of the individual components, that is, of the J-aggregates in solution, and that of the plasmonic nanoparticles in solution, differed from the frequencies obtained from the fits for the J-aggregate and plasmon transitions in the hybrid system. When bound to plasmonic nanoparticles, the J-aggregates exhibited a redshift of 210 cm^{-1}, attributable to structural perturbations of J-aggregates when binding to a metal nanoparticle. The plasmon resonance in the hybrid system was substantially blue shifted with respect to the bare nanoparticles due to small structural differences arising from the surface stabilization properties afforded by the different molecular covering (citrate and polyvinylpyrrolidone for Ag nanoprisms and TDBC for plexcitons). We observed that the frequency of the plasmon in the plexciton system blue shifted over the course of several weeks. It occurred on a time scale much longer than a single experiment and we expect this to have a small effect on the dynamics observed.[41] From the absorption fits, we could see that the plasmon carried most of the transition dipole moment amplitude ($\mu_{J_1 g} = 0.05\mu_{p_1 g}$), justifying the approximation of Delga et al.,[58] of considering that only the plasmonic transition couples to the external radiation field. The dephasing times of the plasmon and J-aggregate in the hybrid system were larger than those for the individual components in solution (1.6 versus 3 fs for plasmon, 34 versus 44 fs for J-aggregates) hinting at a contribution from interfacial processes. The Rabi splitting value extracted from the measured plexciton spectrum was 12% of the molecular transition frequency, placing the system in the ultrastrong coupling regime with respect to the transition frequencies, but not the dephasing rates. Thus, we did not expect Rabi oscillations in the spectra although the splitting was apparent.

With this understanding of the energy states and their line shapes, we turned to the excitation dynamics picture provided by 2DES.

Table 1. Fit parameters for the linear optical response

Separate components in solution[a]

	10^3 cm^{-1}	fs
J-Aggregate		
$\tilde{\nu}_{J1}$	17.04	–
γ_{J1}^{-1}	–	44
Plasmon		
$\tilde{\nu}_{P1}$	16.92	–
γ_{P1}^{-1}	–	3

Hybrid system in solution[b]

	Local		Global	
	10^3 cm^{-1}	fs	10^3cm^{-1}	fs
Site basis				
$\tilde{\nu}_{J1}$	16.83	–	16.08	–
γ_{J1}^{-1}	–	34	–	–
$\tilde{\nu}_{P1}$	19.22	–	19.52	–
γ_{P1}^{-1}	–	1.6	–	–
V_1	0.98	–	0.98	–
Plexcitonic basis				
$\tilde{\nu}_{LB}$	16.67	–	16.42	–
γ_{LB}^{-1}	–	15	–	11
$\tilde{\nu}_{UB}$	19.38	–	19.59	–
γ_{UB}^{-1}	–	1.7	–	2.1

[a]Parameters of the radiative transitions of the individual components in solution (J-aggregates and plasmons measured separately). The absorption line shape is fit with a Lorentzian (see supplemental information for fits).

[b]Parameters for the radiative transition of plexcitons. The spectrum is fit using Equation 2 (global approach) or (3) (local approach). The upper and lower branch properties are obtained by the diagonalization of the Hermitian Hamiltonian of Equation 1 (without dephasing) for the global approach, and of the non-Hermitian Hamiltonian (with dephasing) for the local approach. Dephasing of the branches for the global approach is added in the calculation of the absorption spectrum while for the local approach it is included in the Hamiltonian.

Time-resolved signals

We measured the 2D spectra of the three systems at different population times (referred here as t_2[69]) to obtain the excited-state dynamics of J-aggregates and plasmons, as well as plexcitons in order to disentangle the contributions to dissipation from the metallic and molecular components in the hybrid system (Figure 2).

J-aggregates

The 2D spectra of J-aggregates showed a broad excited-state absorption contribution (ESA, negative, blue) almost coincident with a ground-state bleach (GSB, positive, red) and stimulated emission (SE, positive, red) signal, indicating a near isoenergetic gap between the ground state and first excited-state band, and between the first and second excited-state bands (see Figures 2 and S3 and Note S2). This is in accordance with the previous measurements[56,70,71] and justifies the energy level scheme of Figure 1A. The population of the excited state decayed with very little spectral shift and could be fitted with three lifetimes of 80 ± 20 fs (43%), 4.2 ± 0.4 ps (47%), and a very long time, corresponding to excited-state lifetime (> 100 ps, 10%) (see Figure S4). Those agreed with the time constants obtained from previous transient absorption experiments that have assigned the first component to relaxation into dark exciton states, the second component—to exciton-exciton annihilation (few ps, which depends on the excitation density), and the long-lived component—to relaxation back to the ground state.[56,70,71] The amplitude of the fastest component (close to half of the total signal) was consistent with the loss of

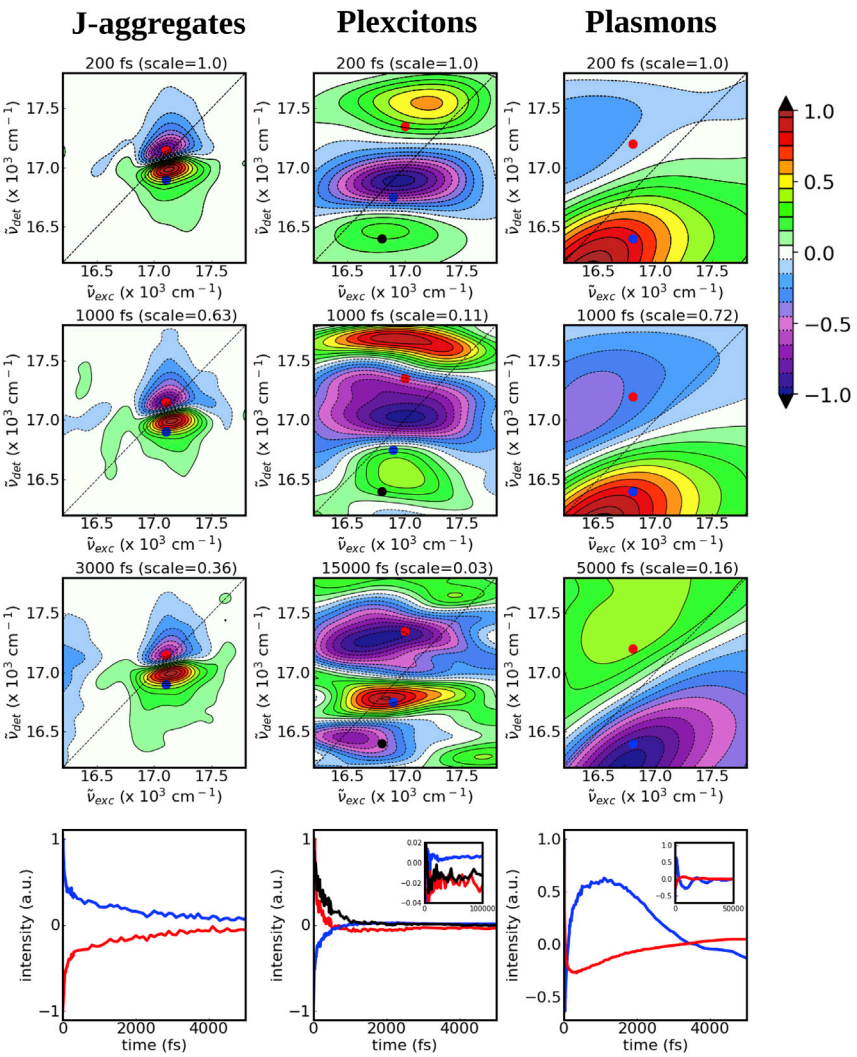

Figure 2. 2D spectra of J-aggregates, plasmons, and plexcitons

2D spectra at different population times t_2, as well as amplitude time traces for J-aggregates, plexcitons, and plasmons (lowest row) at the points indicated in the 2D spectra above. Insets for plexcitons and plasmons show the late-time signals. The data are shown in normalized color scale with the scaling factor shown in parenthesis.

the SE pathway during the waiting time t_2 due to the transition to dark states. In J-aggregates, the dark states were lying above the bright transition such that only the levels within a thermal energy were accessible.

Plasmons

The 2D spectra of Ag nanoparticles showed a single nodal line delimiting negative and positive spectral region (Figure 2). The dynamics were characterized by spectral shifts and sign reversals across this nodal line, and could be separated into the early time dynamics (t_2<4 ps) dominated by electron-electron (e-e) and electron-phonon (e-ph) scattering, and late-time dynamics (t_2>4 ps) corresponding to hot-lattice ground-state relaxation.[41,72–75] We can think of the early time dynamics as corresponding to the processes that transfer the energy from the initial electronic excitation to the lattice, and the late-time dynamics—as the response of the lattice to the excess energy, notably, lattice expansion due to the increase in temperature and the

excitation of acoustic phonon modes.[41] We started analyzing the plasmon data at $T = 100$ fs after the spatial modulation of the index of refraction imposed by the exciting pulses disappeared.[75] The evolution of the signal could be very well fit by a phenomenological equation analogous to the two-temperature model (see Sun et al.[76] and Link et al.,[77] and Note S3, Figures S5–S9):

$$I(t) = A_1\left(1 - e^{-t/\tau_{ee}}\right)e^{-t/\tau_{eph}} + A_2\left(1 - e^{-t/\tau_{eph}}\right)e^{-t/\tau_{phph}} + A_3\left(1 - e^{-t/\tau_{eph}}\right)e^{-t/\tau_{vib}}\cos(\omega_0 t - \varphi) + A_4\left(1 - e^{-t/\tau_{eph}}\right)e^{-t/\tau_{vib}} \quad \text{(Equation 4)}$$

where $\tau_{ee} = 300 \pm 200$ fs, $\tau_{eph} = 1.4 \pm 0.2$ ps are the inferred e-e and e-ph scattering times, $\omega_0 = 2\pi/17.0$ rad/ps^{--1} is the angular frequency of the phonon (breathing mode), $\varphi = 25^o$—its phase, and $\tau_{vib} = 15$ ps—its dephasing time. The thermalization time of the silver nanoparticle with the environment on the time scale of the phonon-phonon scattering time τ_{phph} is longer than the measured population time range (> 1 ns). The asymptotic phase φ of the breathing mode carries information on the excitation mechanism of the acoustic phonon mode. The extracted 25° phase is in a reasonable agreement with the thermal expansion mechanism (predicted at $\varphi = arctan(\omega_0\tau_{e-ph}) = 28°$) and constitutes a signature that energy is dissipated inside the metal nanoparticle, as opposed to evidence of a strong excited electron pressure (see Note S3.3).[78]

Plexcitons

The early time 2D spectra of the plexcitons consisted of two positive regions identifiable with the upper and lower branches, flanking a negative feature (Figure 2). The time evolution of the signal can be well fit by the sum of four exponential decays with time constants of $\tau_d = 40 \pm 20$ fs, $\tau_{ee} = 400 \pm 100$ fs, $\tau_{eph} = 1.6 \pm 0.6$ ps, and $\tau_{solvent} >$ 1 ns, where the last signal appears as a constant background at long times in our measurements. The shortest time constant carries the largest amplitude (> 50%) and corresponds to a pure decay without any appreciable spectral diffusion (see Note S4 and Figures S10–S13). The second and third time constants correspond to pronounced spectral shifts and the 2D spectra show little evolution after this. The time traces (Figure 2, last row) also exhibit fast oscillations on top of the exponential decays, with dominant wavenumbers of 675 and 1,200 cm^{-1}. These correspond to the Raman modes observed in the surface-enhanced Raman spectroscopy measurements of the same plexciton system (see Figure S14,[54]). We left a detailed discussion of the mechanisms behind each time constant for after an analysis of the simulations of the 2DES experiments.

Simulations of the plexciton 2D spectra

We simulated the third-order response for very early times and very late times (Figure 3 and S15–S20 and Tables S1–S4 and Note S5 for details of the simulations). For very early times (i.e., at times much shorter than the e-e scattering time), we considered that the optical response contribution from the non-equilibrium electrons inside the metal to be negligible. At very late times when all excitations have decayed back to the electronic ground state, all the excitations of the system happened from the equilibrium Fermi distribution. The intermediate times were not simulated here, and required an involved model based on Boltzmann equations, which is beyond the scope of this study.

At early times, we followed work on infrared cavities[27] and modeled the nonlinearity of the plexcitons as a Rabi contraction of the excited state. Here the probe pulse examines a system with a fraction f of the total number N of molecules per nanoparticle already excited, thus resulting in a smaller ground state Rabi splitting $\propto \sqrt{(1-f)N}$.

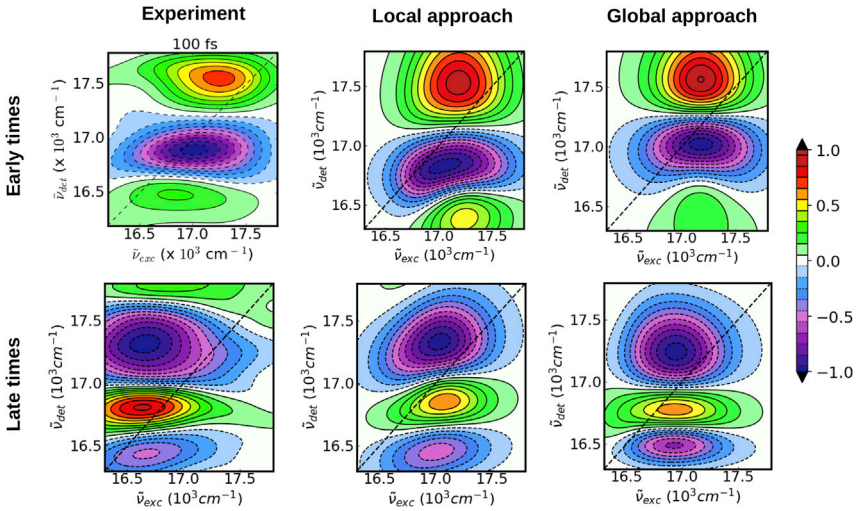

Figure 3. 2DES simulations

Measured and simulated 2D spectra of plexcitons at early (t_2 = 0) and late times. The simulations were carried out both in the local and global approach. Although both approaches give a similar fit to the 2D spectra, the local approach fits the linear absorption much better.

We found that we need to account for the excitation-induced dephasing (EID) and excitation-induced shifts (EIS) as well. We neglected the contributions of interaction pathways that evolve in the excited state during t_2 as the polariton branches decay into intraband metal excitations or molecular dark states shortly after excitation, and these do not have radiative transitions. The late-time simulations assumed that the probe pulse examines an electronic ground state with a hot lattice and therefore a red-shifted plasmon transition, as has been reported for bare metals.[41] We found that while this model reproduces the positive and negative regions of the spectrum, lower values of the plasmon transition strength need to be used (details of the simulations and parameters of the fit are found in the Note S5 and Tables S1–S4.)

We first noticed that the absence of the upper and lower branch structure along the excitation dimension, both at early and late times, is well explained by the finite bandwidth of the pulses. There is a large parameter space that can explain the experimental data both in the local and global approaches, so that experiments with broadband pulses will be needed in the future studies in order to extract unambiguous values of the parameters. Nonetheless, simulations support our assignment of the upper and lower polariton branches as the two positive signals at early times. Similar to modeling of linear absorption, sharper features can be seen with the local approach along the excitation dimension, as is apparent in the broadband simulations (see Figures S17 and S18). At late times, our simulations suggest the presence of a hot ground state. In this case, only the local approach reproduced the positive and negative features observed in the experiment (2 positive, 2 negative) while the global approach could only explain some (2 negative, 1 positive, see Figures S19 and S20).

DISCUSSION

We then analyzed each of the four components of the plexciton decay dynamics (labeled d, ee, eph, and ph-ph) and justified their assignment (see Figure 4). Our analysis is based on the relaxation time constants, the 2D spectral signatures and the overall cohesiveness of the proposed dissipation mechanisms. We note that

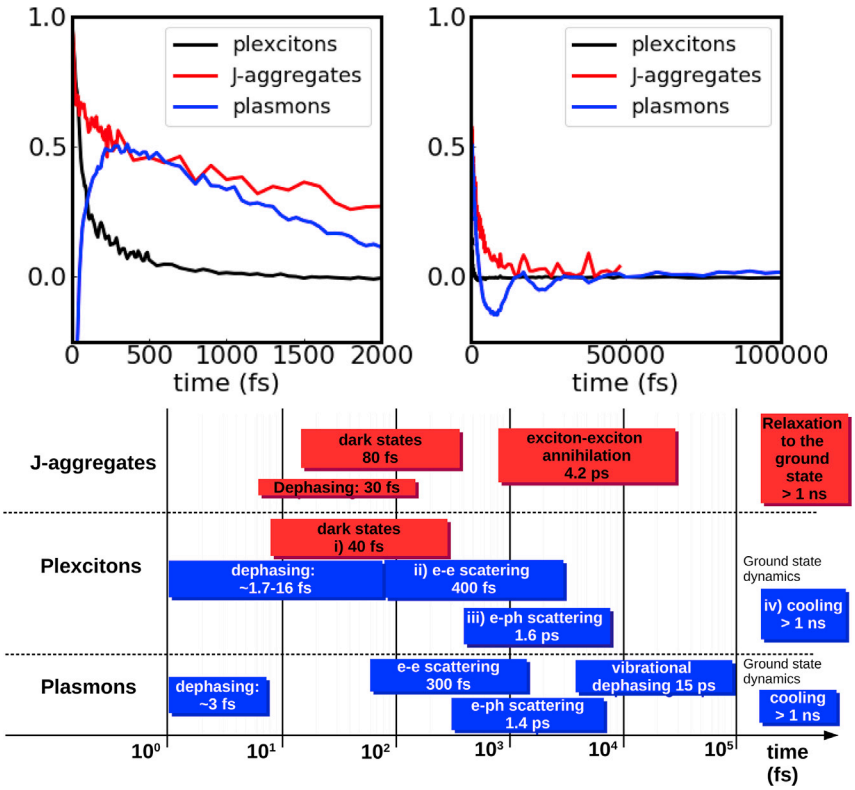

Figure 4. Summary of dynamics

Top panel: representative kinetic traces of J-aggregates (marked by the blue dot in Figure 2, J-aggregate spectra), plasmons (marked by the blue dot in Figure 2, plasmon spectra) and plexcitons (lower branch, marked by the black dot in Figure 2, plexciton spectra) at short and long times. Bottom panel: summary of the time constants measured in the experiments. The bars for a given time constant τ are drawn from $\tau/5$ to 5τ. Vibrational dephasing also exists in plexcitons, however, the energy deposited inside the metallic nanoparticle is insufficient to launch an acoustic mode, so that the rate of this process cannot be measured in our plexciton experiments.

the dephasing rate of the optical coherence is not measured directly but inferred from the absorption line shape, as discussed in the first section of the manuscript.

The signature of the first time constant $\tau_d = 40$ fs is that of pure decay without any spectral shift and appears mainly in the upper polariton branch region (see Figure S11). The J-aggregate has an ultrafast component <100 fs that does not cause any spectral shift either (corresponding to transfer to dark states) and both simulations as well as experiments in microcavities have noted that this very fast transfer to dark states occurs mostly from the upper branch, as we also observe.[79–81] However, the amplitude of this fast component in plexcitons exceeds 50% of the total signal so that it cannot be explained exclusively by transfer to dark states, which would entail a suppression of the SE pathway, but likely includes some relaxation of electrons to the ground state. In plasmons, a spatial long-range order imposed by the laser sequence produces a strong distortion and variation of the signal at very early times.[75] In our plasmonic nanoparticles, the first 100 fs were dominated by this spatial order, however, the spectral distortion of this process were absent in plexcitons, and hence, it is doubtful whether the same process occurs in the decorated nanoparticles. Another possibility is that of radiation damping of the plasmon transition that leads to recombination to the ground state. This mechanism is likely to be unchanged in bare or TDBC-decorated Ag nanoparticles. We thus propose that this fast decay

component corresponds to a combination of radiation damping and transfer to J-aggregate dark states, predominantly from the upper branch. During the second component τ_{ee} (400 fs) we saw a pronounced spectral shift. The fact that J-aggregates have no processes that induce a spectral shift, while plasmons do, and with a similar time constant (300 fs), suggests that this process corresponds to the e-e scattering inside the metal nanoparticle. Unlike EIS, mentioned previously, which occurs almost instantaneously, the shift discussed here develops on the time scale of electron-electron scattering. The constant background at very long times is assigned to a hot lattice plexciton signal (see Figures 3, S13, S19, and S20 and Note S5), so that the process that extends beyond the time range of the instrument (>1 ns) is likely thermalization of the solvent via phonon-phonon scattering with the time τ_{ph-ph}. Previous measurements set this process in the hundreds of ps.[82] The third component τ_{eph} (1.6 ps) induced a small spectral shift. The time constant for this process was close to the time constant for e-ph scattering measured in the Ag nanoprisms (1.4 ps) and suggested the same underlying process. This tentative assignment was bolstered by the presence of a hot lattice after this process was over. Alternate assignments of this third time constant would require an alternate mechanism for warming the lattice; however, warming via the adsorbed molecules is not likely as this process is governed by τ_{ph-ph} and would also require several hundreds of ps. It is also striking that the replenishing of the lower polariton by the dark state reservoir was absent (contrary to microcavities[80]) and that the long-lived dark modes did not survive after a few ps. In fact, the lower polariton dynamics seem to be determined by τ_{ee} and τ_{eph}, and we attribute this to the direct coupling between molecules and the metallic surface, which likely connects the relaxation of TDBC dark states with that of the non-equilibrium electron distribution inside the lattice. Lastly, we mention that a signature of exciton-exciton annihilation—corresponding to a pure decay of the signal—was not observed, although we cannot rule out that it is a process that contributes to the third time constant.

Our measurements suggest that enough energy is dissipated outside of the metal nanoparticle so that the acoustic phonon cannot be excited to a detectable intensity. It is most likely dissipated in the J-aggregates with possible contributions from the surface, given the fast transfer rate to dark states, which can compete with e-e and e-ph scattering. While the coherence of the plexciton is limited by processes inside the metal, the energy dissipation would thus be strongly influenced by ultrafast processes inside the J-aggregates. This indicates that to increase the lifetime of the excitation we should first modify the molecular component, for example, by going toward the single molecule limit where the number of dark states is significantly reduced and isolating the molecules from the metal so that recombination via surface processes is suppressed.

Furthermore, the observation that e-e scattering events exist in plexcitons reveals a crucial point in plasmon-based polariton systems: that one can no longer speak exclusively in terms of upper or lower branches once dephasing processes have transformed the initial coherent excitation into a non-equilibrium distribution of electrons and holes. A framework beyond Rabi type Hamiltonians, including the continuum states of the metallic band is needed in order to describe anything other than the early or late times. Our findings are different from microcavity dynamics as much of the signal arises from the non-equilibrium distribution of electronic excitations inside the metal. Whereas the direct interaction between molecules and silver surface excitations of microcavities is virtually inexistent (because the mirrors are usually coated by an insulating polymer layer and the cavity mode antinode lies inside the cavity), there is strong coupling between molecules and the silver surface in our samples that is beyond the dipolar coupling of the bright molecular and plasmon

transitions as evidenced by the short lifetimes of the TDBC dark states. Thus, metallic excitations can directly exchange energy and likely charge with adsorbed molecules. The possibilities afforded by this interaction in terms of hot electron chemistry set apart plasmon- from microcavity-based polariton states.

Many possible applications of atomic cQED systems have been explored throughout the years, from basic tests of quantum mechanics and quantum information processing to studies of strong light-matter coupling, its usefulness has been proven many times over. In contrast, the field of molecular cQED systems—and more so when the cavity is substituted by a plasmonic mode—is relatively recent. We are still learning what these systems are capable of and in what ways they differ from the more traditional cQED versions. There are many interesting phenomena: delocalization, collective behavior, chemical reactivity, and remote energy transfer.[5–16,19–28] In our work, we show that we need to understand the basic excitation dynamics occurring in metals when these are strongly coupled to molecules. The stronger coupling of a plasmon to its bath than to J-aggregates means that the site states are dressed by the dissipative modes. The resulting spectrum and underlying phenomenon is more akin to an interference-type process than a Rabi splitting.[83] This type of physics has been recognized before in scattering settings;[84,85] however, it has not been connected to the local versus global approach to Markovian master equations. As we show in this work, taking the local approach requires an extension to non-Hermitian Hamiltonians in the response function formalism. Thus, our study provides both the motivation and groundwork to study the nonlinear response of Markovian systems in the limit of large dissipation that dominates plasmonic materials. We believe that given the short coherence times in colloidal suspensions of localized surface plasmon materials, a very interesting application of plexcitons arises in the manipulation of optical transitions to favor charge transfer to an acceptor, or to promote catalysis, as opposed to performing coherent operations with these states.

Conclusion

We have presented a systematic study of plexciton dynamics using linear and third-order optical response. We were able to explain the line shapes using a non-Hermitian Hamiltonian extension of response function formalism, which are rooted in the local approach to Markovian master equations. We have tracked the excitation evolution and identified one dephasing and four relaxation time scales, which we have attributed to either molecular-like or metallic-like processes. Remarkably, we find that a significant part of the energy is dissipated outside of the metal lattice. Our work suggests that when considering the relaxation of plexcitons a more nuanced version of the dynamics in terms of hot electron distributions is needed.

Realizations of polaritonic systems continue to bring new insights into basic quantum physics concepts and emergent behavior of hybrid systems. Because the plasmon-based polaritons exists at the intersection of strong light-matter coupling and important condensed matter and chemical processes, such as interfacial charge transfer and photocatalysis, they are uniquely fit to bring desirable features of the former into the societally relevant applications of the latter.

EXPERIMENTAL PROCEDURES

Resource availability

Lead contact

Further information and requests for additional details should be directed to and will be fulfilled by the Lead Contact, Donatas Zigmantas (donatas.zigmantas@chemphys.lu.se).

Materials availability

This study did not generate new unique reagents.

Data and code availability

The data and code are available from the Lead Contact, Donatas Zigmantas upon reasonable request.

Synthesis

We synthesized plasmonic and plexcitonic nanoparticles as reported in our earlier studies.[38,54] Briefly, the Ag nanoprisms with varying edge lengths were wet-chemically synthesized by using a seed-mediated protocol. Initially, isotropic seed Ag nanoparticles were synthesized, which was then followed by a slower growth of anisotropic Ag nanoprisms. By controlling the number of seed nanoparticles in the growth solution, the size of the nanoprisms can be easily tuned. Concurrently, the localized surface plasmon polariton frequency of the nanoparticles vary from 400 to 1,100 nm. Plexcitonic nanoparticles used in this study were synthesized by self-assembly of a J-aggregate dye (TDBC, 5,5,6,6-tetrachloro-di(4-sulfobutyl) benzimidazolocarbocyanine, FEW Chemicals) on Ag nanoprism surfaces. It should be noted that the excess dye molecules were removed by centrifugation.

Two-dimensional electronic spectroscopy

The 2DES spectrometer is described in detail in Augulis and Zigmantas.[86] Briefly, femtosecond broadband pulses were generated by feeding the 1,030 nm output of a Pharos laser (Light Conversion) to a noncollinear optical parametric amplifier (Light Conversion) to generate a pulse at 590 nm. The narrow-band spectrum (see Figure S15, simulations) where generated by compressing the pulse using chirped mirrors and a prism compressor, and subsequently limiting the spectrum using a blade edge to obtain a 40 nm FWHM pulse of less than 25 fs duration (used for J-aggregates and plexcitons measurements). To obtain the broadband pulse we used a home-built pulse shaper arranged in a folded 4f-geometry. The setup is based on a dual liquid crystal spatial light modulator (SLM-S640d, Jenoptik) enabling simultaneous shaping of phase and amplitude.[87] Second order dispersion from material in the beam path is for the most part compensated for by a pair of chirped mirrors in combination with a prism compressor consisting of two fused silica prisms at a separation of 310 mm. Higher order phase distortions are compensated for by the pulse shaper. With this arrangement broadband pulses with a duration of 11 fs were obtained (used for the Ag nanoparticles measurement). All four beams are focused at the sample to the spot size of 160 μm. The pulses were attenuated to pulse energies in the range of 0.1 to 1.25 nJ/pulse. Polarizations of pulses 1 and 2 were set to magic angle with respect to pulse 3 and the detected signal polarization. Several measurement series were carried out across population times. The coherence time was scanned from −71.6 to 151.2 fs in 1.4 fs steps for J-aggregates, from -42 to 63 fs for plasmons and from −50.4 to 50.4 fs for plexcitons. The resolution of the measurement was 60 cm^{-1} at the detection frequency and 290 cm^{-1} at the excitation frequency.

SUPPLEMENTAL INFORMATION

Supplemental Information can be found online at https://doi.org/10.1016/j.chempr.2021.02.028.

ACKNOWLEDGMENTS

Funding is acknowledged from the European Union through the Marie Sklodowska-Curie Grant Agreement no. 702694, from Nanolund and from Swedish Research Council grants

2017-05150, 2017-04344, and 2018-05090. We also acknowledge stimulating discussions with Patrick Potts.

AUTHOR CONTRIBUTIONS

D.F.-S. and D.Z. conceived the idea. D.F.-S., L.W., I.M., and D.Z. designed and performed the experiments. D.F.-S., P.-A.M., and T.P. discussed the theory and D.F.-S. carried out the simulations. S.S. and S.B. synthesized the samples. D.F.-S. and P.-A.M. analyzed the data and D.F.-S. wrote the manuscript, edited by P.-A.M., T.P., and D.Z., with input from all the other authors.

DECLARATION OF INTERESTS

The authors declare no competing interests.

Received: March 30, 2020
Revised: November 11, 2020
Accepted: February 24, 2021
Published: March 26, 2021

REFERENCES

1. Walther, H., Varcoe, B.T.H., Englert, B.-G., and Becker, T. (2006). Cavity quantum electrodynamics. Rep. Prog. Phys. *69*, 1325–1382.

2. Mabuchi, H., and Doherty, A.C. (2002). Cavity quantum electrodynamics: coherence in context. Science *298*, 1372–1377.

3. Haroche, S., and Kleppner, D. (1989). Cavity quantum electrodynamics. Phys. Today *42*, 24–30.

4. Raimond, J.M., Brune, M., and Haroche, S. (2001). Manipulating quantum entanglement with atoms and photons in a cavity. Rev. Mod. Phys. *73*, 565–582.

5. Kasprzak, J., Richard, M., Kundermann, S., Baas, A., Jeambrun, P., Keeling, J.M.J., Marchetti, F.M., Szymańska, M.H., André, R., Staehli, J.L., et al. (2006). Bose-Einstein condensation of exciton polaritons. Nature *443*, 409–414.

6. Martínez-Martínez, L.A., Du, M., F Ribeiro, R., Kéna-Cohen, S., and Yuen-Zhou, J. (2018). Polariton-assisted singlet fission in acene aggregates. J. Phys. Chem. Lett. *9*, 1951–1957.

7. Yuen-Zhou, J., Saikin, S.K., Zhu, T., Onbasli, M.C., Ross, C.A., Bulovic, V., and Baldo, M.A. (2016). Plexciton Dirac points and topological modes. Nat. Commun. *7*, 11783.

8. Zhong, X., Chervy, T., Wang, S., George, J., Thomas, A., Hutchison, J.A., Devaux, E., Genet, C., and Ebbesen, T.W. (2016). Non-radiative energy transfer mediated by hybrid light-matter states. Angew. Chem. Int. Ed. Engl. *55*, 6202–6206.

9. Feist, J., and Garcia-Vidal, F.J. (2015). Extraordinary exciton conductance induced by strong coupling. Phys. Rev. Lett. *114*, 196402.

10. Schachenmayer, J., Genes, C., Tignone, E., and Pupillo, G. (2015). Cavity-enhanced transport of excitons. Phys. Rev. Lett. *114*, 196403.

11. Herrera, F., and Spano, F.C. (2016). Cavity-controlled chemistry in molecular ensembles. Phys. Rev. Lett. *116*, 238301.

12. Galego, J., Garcia-Vidal, F.J., and Feist, J. (2015). Cavity-induced modifications of Molecular Structure in the strong-coupling regime. Phys. Rev. X *5*, 041022.

13. Hutchison, J.A., Liscio, A., Schwartz, T., Canaguier-Durand, A., Genet, C., Palermo, V., Samorì, P., and Ebbesen, T.W. (2013). Tuning the work-function via strong coupling. Adv. Mater. *25*, 2481–2485.

14. Hutchison, J.A., Schwartz, T., Genet, C., Devaux, E., and Ebbesen, T.W. (2012). Modifying chemical landscapes by coupling to vacuum fields. Angew. Chem. Int. Ed. Engl. *51*, 1592–1596.

15. Thomas, A., George, J., Shalabney, A., Dryzhakov, M., Varma, S.J., Moran, J., Chervy, T., Zhong, X., Devaux, E., Genet, C., et al. (2016). Ground-state chemical reactivity under vibrational coupling to the vacuum electromagnetic field. Angew. Chem. Int. Ed. Engl. *55*, 11462–11466.

16. Wang, S., Mika, A., Hutchison, J.A., Genet, C., Jouaiti, A., Hosseini, M.W., and Ebbesen, T.W. (2014). Phase transition of a perovskite strongly coupled to the vacuum field. Nanoscale *6*, 7243–7248.

17. Mandal, A., and Huo, P. (2019). Investigating new reactivities enabled by polariton photochemistry. J. Phys. Chem. Lett. *10*, 5519–5529.

18. Manuel, A.P., Kirkey, A., Mahdi, N., and Shankar, K. (2019). Plexcitonics – fundamental principles and optoelectronic applications. J. Mater. Chem. C *7*, 1821–1853.

19. Coles, D.M., Somaschi, N., Michetti, P., Clark, C., Lagoudakis, P.G., Savvidis, P.G., and Lidzey, D.G. (2014). Polariton-mediated energy transfer between organic dyes in a strongly coupled optical microcavity. Nat. Mater. *13*, 712–719.

20. Sáez-Blázquez, R., Feist, J., Fernández-Domínguez, A.I., and García-Vidal, F.J. (2018). Organic polaritons enable local vibrations to drive long-range energy transfer. Phys. Rev. B *97*, 241407.

21. Xiang, B., Ribeiro, R.F., Du, M., Chen, L., Yang, Z., Wang, J., Yuen-Zhou, J., and Xiong, W. (2020). Intermolecular vibrational energy transfer enabled by microcavity strong light–matter coupling. Science *368*, 665–667.

22. Du, M., Martínez-Martínez, L.A., Ribeiro, R.F., Hu, Z., Menon, V.M., and Yuen-Zhou, J. (2018). Theory for polariton-assisted remote energy transfer. Chem. Sci. *9*, 6659–6669.

23. Zhong, X., Chervy, T., Zhang, L., Thomas, A., George, J., Genet, C., Hutchison, J.A., and Ebbesen, T.W. (2017). Energy transfer between spatially separated entangled molecules. Angew. Chem. Int. Ed. Engl. *56*, 9034–9038.

24. Krainova, N., Grede, A.J., Tsokkou, D., Banerji, N., and Giebink, N.C. (2020). Polaron photoconductivity in the weak and strong light-matter coupling regime. Phys. Rev. Lett. *124*, 177401.

25. Du, M., Ribeiro, R.F., and Yuen-Zhou, J. (2019). Remote control of chemistry in optical cavities. Chem *5*, 1167–1181.

26. Fregoni, J., Granucci, G., Persico, M., and Corni, S. (2020). Strong coupling with light enhances the photoisomerization quantum yield of azobenzene. Chem *6*, 250–265.

27. F Ribeiro, R., Dunkelberger, A.D., Xiang, B., Xiong, W., Simpkins, B.S., Owrutsky, J.C., and Yuen-Zhou, J. (2018). Theory for nonlinear spectroscopy of vibrational polaritons. J. Phys. Chem. Lett. *9*, 3766–3771.

28. Feist, J., Galego, J., and García-Vidal, F.J. (2018). Polaritonic chemistry with organic molecules. ACS Photonics *5*, 205–216.

29. Törmä, P., and Barnes, W.L. (2015). Strong coupling between surface plasmon polaritons

and emitters: a review. Rep. Prog. Phys. *78*, 013901.

30. Flick, J., Rivera, N., and Narang, P. (2018). Strong light-matter coupling in quantum chemistry and quantum photonics. Nanophotonics *7*, 1479–1501.

31. Ebbesen, T.W. (2016). Hybrid light-matter states in a molecular and material science perspective. Acc. Chem. Res. *49*, 2403–2412.

32. Chen, X., Chen, Y.H., Qin, J., Zhao, D., Ding, B., Blaikie, R.J., and Qiu, M. (2017). Mode modification of plasmonic gap resonances induced by strong coupling with molecular excitons. Nano Lett *17*, 3246–3251.

33. Wersäll, M., Cuadra, J., Antosiewicz, T.J., Balci, S., and Shegai, T. (2017). Observation of mode splitting in photoluminescence of individual plasmonic nanoparticles strongly coupled to molecular excitons. Nano Lett *17*, 551–558.

34. Roller, E.M., Argyropoulos, C., Högele, A., Liedl, T., and Pilo-Pais, M. (2016). Plasmon–exciton coupling using DNA templates. Nano Lett *16*, 5962–5966.

35. Antosiewicz, T.J., Apell, S.P., and Shegai, T. (2014). Plasmon–exciton interactions in a core–shell geometry: From enhanced absorption to strong coupling. ACS Photonics *1*, 454–463.

36. Sugawara, Y., Kelf, T.A., Baumberg, J.J., Abdelsalam, M.E., and Bartlett, P.N. (2006). Strong coupling between localized plasmons and organic excitons in metal nanovoids. Phys. Rev. Lett. *97*, 266808.

37. Bellessa, J., Bonnand, C., Plenet, J.C., and Mugnier, J. (2004). Strong coupling between surface plasmons and excitons in an organic semiconductor. Phys. Rev. Lett. *93*, 036404.

38. Balci, S., Kucukoz, B., Balci, O., Karatay, A., Kocabas, C., and Yaglioglu, G. (2016). Tunable Plexcitonic nanoparticles: a model system for studying plasmon–exciton interaction from the weak to the ultrastrong coupling regime. ACS Photonics *3*, 2010–2016.

39. Santhosh, K., Bitton, O., Chuntonov, L., and Haran, G. (2016). Vacuum Rabi splitting in a plasmonic cavity at the single quantum emitter limit. Nat. Commun. *7*, ncomms11823.

40. Hertzog, M., Wang, M., Mony, J., and Börjesson, K. (2019). Strong light-matter interactions: a new direction within chemistry. Chem. Soc. Rev. *48*, 937–961.

41. Voisin, C., Del Fatti, N., Christofilos, D., and Vallée, F. (2001). Ultrafast electron dynamics and optical nonlinearities in metal nanoparticles. J. Phys. Chem. B *105*, 2264–2280.

42. Lin, Y., Gaebler, J.P., Reiter, F., Tan, T.R., Bowler, R., Sørensen, A.S., Leibfried, D., and Wineland, D.J. (2013). Dissipative production of a maximally entangled steady state of two quantum bits. Nature *504*, 415–418.

43. Scully, M.O., Chapin, K.R., Dorfman, K.E., Kim, M.B., and Svidzinsky, A. (2011). Quantum heat engine power can be increased by noise-induced coherence. Proc. Natl. Acad. Sci. USA *108*, 15097–15100.

44. Fofang, N.T., Grady, N.K., Fan, Z., Govorov, A.O., and Halas, N.J. (2011). Plexciton dynamics: exciton-plasmon coupling in a J-aggregate-Au nanoshell complex provides a mechanism for nonlinearity. Nano Lett *11*, 1556–1560.

45. Balci, S., Kocabas, C., Küçüköz, B., Karatay, A., Akhüseyin, E., Gul Yaglioglu, H.G., and Elmali, A. (2014). Probing ultrafast energy transfer between excitons and plasmons in the ultrastrong coupling regime. Appl. Phys. Lett. *105*, 051105.

46. Hranisavljevic, J., Dimitrijevic, N.M., Wurtz, G.A., and Wiederrecht, G.P. (2002). Photoinduced charge separation reactions of J-aggregates coated on silver nanoparticles. J. Am. Chem. Soc. *124*, 4536–4537.

47. Vasa, P., Wang, W., Pomraenke, R., Lammers, M., Maiuri, M., Manzoni, C., Cerullo, G., and Lienau, C. (2013). Real-time observation of ultrafast Rabi oscillations between excitons and plasmons in metal nanostructures with J-aggregates. Nat. Photonics *7*, 128–132.

48. Wiederrecht, G.P., Wurtz, G.A., and Bouhelier, A. (2008). Ultrafast hybrid plasmonics. Chem. Phys. Lett. *461*, 171–179.

49. Hoang, T.B., Akselrod, G.M., and Mikkelsen, M.H. (2016). Ultrafast room-temperature single photon emission from quantum dots coupled to plasmonic nanocavities. Nano Lett *16*, 270–275.

50. Xiang, B., Ribeiro, R.F., Dunkelberger, A.D., Wang, J., Li, Y., Simpkins, B.S., Owrutsky, J.C., Yuen-Zhou, J., and Xiong, W. (2018). Two-dimensional infrared spectroscopy of vibrational polaritons. Proc. Natl. Acad. Sci. USA *115*, 4845–4850.

51. Zhang, Z., Wang, K., Yi, Z., Zubairy, M.S., Scully, M.O., and Mukamel, S. (2019). Polariton-assisted cooperativity of molecules in microcavities monitored by two-dimensional infrared spectroscopy. J. Phys. Chem. Lett. *10*, 4448–4454.

52. DelPo, C.A., Kudisch, B., Park, K.H., Khan, S.U., Fassioli, F., Fausti, D., Rand, B.P., and Scholes, G.D. (2020). Polariton transitions in femtosecond transient absorption studies of ultrastrong light-molecule coupling. J. Phys. Chem. Lett. *11*, 2667–2674.

53. Mewes, L., Wang, M., Ingle, R.A., Börjesson, K., and Chergui, M. (2020). Energy relaxation pathways between light-matter states revealed by coherent two-dimensional spectroscopy. Commun. Phys. *3*, 157.

54. Balci, S. (2013). Ultrastrong plasmon-exciton coupling in metal nanoprisms with J-aggregates. Opt. Lett. *38*, 4498–4501.

55. Agranovich, V.M., and Malshukov, A.G. (1974). Surface polariton spectra if the resonance with the transition layer vibrations exists. Opt. Commun. *11*, 169–171.

56. Minoshima, K., Taiji, M., Misawa, K., and Kobayashi, T. (1994). Femtosecond nonlinear optical dynamics of excitons in J-aggregates. Chem. Phys. Lett. *218*, 67–72.

57. Milota, F., Prokhorenko, V.I., Mancal, T., von Berlepsch, H., Bixner, O., Kauffmann, H.F., and Hauer, J. (2013). Vibronic and vibrational coherences in two-dimensional electronic spectra of supramolecular J-aggregates. J. Phys. Chem. A *117*, 6007–6014.

58. Delga, A., Feist, J., Bravo-Abad, J., and Garcia-Vidal, F.J. (2014). Theory of strong coupling between quantum emitters and localized surface plasmons. J. Opt. *16*, 114018.

59. Shah, R.A., Scherer, N.F., Pelton, M., and Gray, S.K. (2013). Ultrafast reversal of a Fano resonance in a plasmon-exciton system. Phys. Rev. B *88*, 075411.

60. Zelinskyy, Y., Zhang, Y., and May, V. (2012). Supramolecular complex coupled to a metal nanoparticle: computational studies on the optical absorption. J. Phys. Chem. A *116*, 11330–11340.

61. Varguet, H., Rousseaux, B., Dzsotjan, D., Jauslin, H.R., Guérin, S., and des Francs, G.C.d. (2019). Non-hermitian Hamiltonian description for quantum plasmonics: from dissipative dressed atom picture to Fano states. J. Phys. B: At. Mol. Opt. Phys. *52*, 055404.

62. Piryatinski, A., Roslyak, O., Li, H., and Bittner, E.R. (2020). Nonequilibrium states of a plasmonic Dicke model with coherent and dissipative surface-plasmon–quantum-emitter interactions. Phys. Rev. Research *2*, 013141.

63. Mukamel, S. (1995). Principles of Nonlinear Optical Spectroscopy (Oxford University Press).

64. Hofer, P.P., Perarnau-Llobet, M., Miranda, L.D.M., Haack, G., Silva, R., Brask, J.B., and Brunner, N. (2017). Markovian master equations for quantum thermal machines: local versus global approach. New J. Phys. *19*, 123037.

65. Cho, M. (2009). Two-Dimensional Optical Spectroscopy (CRC Press).

66. Malý, P., and Mančal, T. (2018). Signatures of exciton delocalization and exciton-exciton annihilation in fluorescence-detected two-dimensional coherent spectroscopy. J. Phys. Chem. Lett. *9*, 5654–5659.

67. Wright, O.B. (1994). Ultrafast nonequilibrium stress generation in gold and silver. Phys. Rev. B Condens. Matter. *49*, 9985–9988.

68. Weick, G., Molina, R.A., Weinmann, D., and Jalabert, R.A. (2005). Lifetime of the first and second collective excitations in metallic nanoparticles. Phys. Rev. B *72*, 115410.

69. Jonas, D.M. (2003). Two-dimensional femtosecond spectroscopy. Annu. Rev. Phys. Chem. *54*, 425–463.

70. Lee, J.-H., Min, C.-K., and Joo, T. (2001). Ultrafast optical dynamics of excitons in J-aggregates. J. Chem. Phys. *114*, 377.

71. Sundström, V., Gillbro, T., Gadonas, R.A., and Piskarskas, A. (1988). Annihilation of singlet excitons in J aggregates of pseudoisocyanine (PIC) studied by pico- and subpicosecond spectroscopy. J. Chem. Phys. *89*, 2754–2762.

72. Hu, M., Wang, X., Hartland, G.V., Mulvaney, P., Juste, J.P., and Sader, J.E. (2003). Vibrational response of nanorods to ultrafast laser induced heating: theoretical and experimental analysis. J. Am. Chem. Soc. *125*, 14925–14933.

73. Hartland, G.V. (2011). Optical studies of dynamics in noble metal nanostructures. Chem. Rev. *111*, 3858–3887.

74. Brown, A.M., Sundararaman, R., Narang, P., Schwartzberg, A.M., Goddard, W.A., and Atwater, H.A. (2017). Experimental and ab initio ultrafast carrier dynamics in plasmonic nanoparticles. Phys. Rev. Lett. *118*, 087401.

75. Lietard, A., Hsieh, C.S., Rhee, H., and Cho, M. (2018). Electron heating and thermal relaxation of gold nanorods revealed by two-dimensional electronic spectroscopy. Nat. Commun. *9*, 891.

76. Sun, C.-K., Vallée, F., Acioli, L.H., Ippen, E.P., and Fujimoto, J.G. (1994). Femtosecond-tunable measurement of electron thermalization in gold. Phys. Rev. B Condens. Matter. *50*, 15337–15348.

77. Link, S., Burda, C., Wang, Z.L., and El-Sayed, M.A. (1999). Electron dynamics in gold and gold–silver alloy nanoparticles: the influence of a nonequilibrium electron distribution and the size dependence of the electron–phonon relaxation. J. Chem. Phys. *111*, 1255–1264.

78. Voisin, C., Del Fatti, N.D., Christofilos, D., and Vallée, F. (2000). Time-resolved investigation of the vibrational dynamics of metal nanoparticles. Appl. Surf. Sci. *164*, 131–139.

79. Agranovich, V.M., Litinskaia, M., and Lidzey, D.G. (2003). Cavity polaritons in microcavities containing disordered organic semiconductors. Phys. Rev. B *67*, 085311.

80. Virgili, T., Coles, D., Adawi, A.M., Clark, C., Michetti, P., Rajendran, S.K., Brida, D., Polli, D., Cerullo, G., and Lidzey, D.G. (2011). Ultrafast polariton relaxation dynamics in an organic semiconductor microcavity. Phys. Rev. B *83*, 245309.

81. Groenhof, G., Climent, C., Feist, J., Morozov, D., and Toppari, J.J. (2019). Tracking polariton relaxation with multiscale molecular dynamics simulations. J. Phys. Chem. Lett. *10*, 5476–5483.

82. Del Fatti, N., Voisin, C., Achermann, M., Tzortzakis, S., Christofilos, D., and Vallée, F. (2000). Nonequilibrium electron dynamics in noble metals. Phys. Rev. B *61*, 16956–16966.

83. Finkelstein-Shapiro, D., Viennot, D., Saideh, I., Hansen, T., Pullerits, T.o., and Keller, A. (2020). Adiabatic elimination and subspace evolution of open quantum systems. Phys. Rev. A *101*, 042102.

84. Faucheaux, J.A., Fu, J., and Jain, P.K. (2014). Unified theoretical framework for realizing diverse regimes of strong coupling between plasmons and electronic transitions. J. Phys. Chem. C *118*, 2710–2717.

85. Pelton, M., Storm, S.D., and Leng, H. (2019). Strong coupling of emitters to single plasmonic nanoparticles: exciton-induced transparency and Rabi splitting. Nanoscale *11*, 14540–14552.

86. Augulis, R., and Zigmantas, D. (2011). Two-dimensional electronic spectroscopy with double modulation lock-in detection: enhancement of sensitivity and noise resistance. Opt. Express *19*, 13126–13133.

87. Wittenbecher, L., and Zigmantas, D. (2019). Correction of Fabry-Perot interference effects in phase and amplitude pulse shapers based on liquid crystal spatial light modulators. Opt. Express *27*, 22970–22982.